(Received 18 December 2024, Accepted 23 January 2025, Scheduled 6 February 2025)

A Dual-Polarized Microstrip Patch Antenna with High Port Isolation Based on AMC Surface

Dalong Xu, Wenbo Li, Yan Wang, Hao Wang, and Jianyin Cao*

School of Electronic and Optical Engineering, Nanjing University of Science and Technology, Nanjing 210094, China

ABSTRACT: A high port isolation dual-polarized microstrip patch antenna based on artificial magnetic conductor (AMC) surface is proposed in this paper. The antenna is composed of two stacked patches and H-shaped coupled slots with improved impedance matching bandwidth. The feed network is composed of two orthogonal microstrip feed lines for dual polarizations, and metallic vias are arranged around them to improve the port isolation. The AMC surface is designed and loaded below the feed lines. The electric field coupling between the feeding slots on the ground are reduced, and the port isolation is greatly improved. The simulated results show that the proposed antenna has a port isolation better than 48 dB and a cross-polarization level of −26 dB over the frequency of 9.3–9.5 GHz. Moreover, based on zero-reflection phase characteristic of the AMC, the profile of the antenna is reduced to 7.3 mm ($0.23\lambda_0$, λ_0 is the wavelength at 9.4 GHz). A prototype is fabricated to verify the analysis of proposed antenna. The measured results indicate that a high port isolation better than 44 dB and a cross-polarization level lower than −22 dB are achieved. The maximum gain is higher than 6.98 dBi and 6.5 dBi for the vertical and horizontal polarizations, respectively. With the advantages of high port isolation and low profile, this antenna offers a good candidate for weather radar applications.

1. INTRODUCTION

In recent years, with the development of antenna technology and the abundance of the application environment, spectrum resources are more widely used. Single-polarized antenna can only achieve a single function of receiving or transmitting, which is limited in complex environment. In order to cope with this situation, dual-polarized antenna has become a popular research direction. Dual-polarized antenna can receive or transmit two orthogonal polarized waves at the same time. Dual-polarized antennas have been applied in 5G communication, weather radar, military applications, and other fields with strict requirements on impedance bandwidth, port isolation, and cross-polarization level.

Parasitic patches are added, and feeding method is studied to expand the impendence bandwidth of dual-polarized antennas [1–12]. Slot coupling is one of the most commonly used feeding methods in wideband dual-polarized antennas [4–8]. The biorthogonal bias slots are provided as a relatively simple solution to achieve bandwidth of 15%–24% and port isolation higher than 25 dB. In addition, the impedance bandwidth can be expanded by adding parasitic patches. In [4], a dual-polarized antenna element with aperture coupled feeding technique, working in the frequency range of 2.77 to 3.10 GHz has been designed. The antenna achieves high port isolation and is simple enough for polarimetric weather radar applications. In [5], the impedance bandwidth of a dual-polarized antenna is broadened by parasitic patch and slot coupling. A PEC reflector is placed with a distance of 0.26λ away from the intermediate substrate to suppress the back radiation. The port isolation of the antenna is 23 dB with an overall profile of 0.38λ. However, back radiation is serious due to the existence of the slots. In order to avoid the influence on the gain, it is necessary to add a reflecting plate 0.25λ away from the slot, which will increase the profile of the antenna.

In order to overcome these problems, the AMC surface has become an important research direction. The AMC surface is applied to design ME-dipole antennas with dual polarization performance [13–18]. In [15], the antenna is composed of a pair of cross dipoles and a wideband AMC reflector. The profile is significantly reduced from 22 mm to 12 mm. The simulation results show that the port isolation is 22 dB, and the cross-polarization level is less than −20 dB. In [18], a low-profile antenna applying an AMC structure for base station application is presented. The profile height is only about 19 mm (0.14λ at 2.2 GHz). The measured results show that the port isolation is 25 dB, and the cross-polarization level is lower than −26 dB. It can be seen that it is a challenge for dual-polarized antenna implemented with high port isolation and low cross-polarization at the same time.

In this paper, a dual-polarized microstrip antenna with low profile and high port isolation based on AMC surface is proposed. A wide impedance bandwidth of 12.5%, port isolation better than 48 dB, and cross-polarization level lower than −26 dB are achieved. In addition, the profile height of the antenna is reduced from 9.4 mm ($0.29\lambda_0$) to 7.3 mm ($0.23\lambda_0$). Detailed analysis and the structure of this antenna are shown in the following parts. Section 2 introduces the structure of the antenna and the design of the AMC surface. Section 3 introduces the simulated and measured results of the antenna, and the conclusion is shown in Section 4.

* Corresponding author: Jianyin Cao (jianyin.cao@njust.edu.cn).

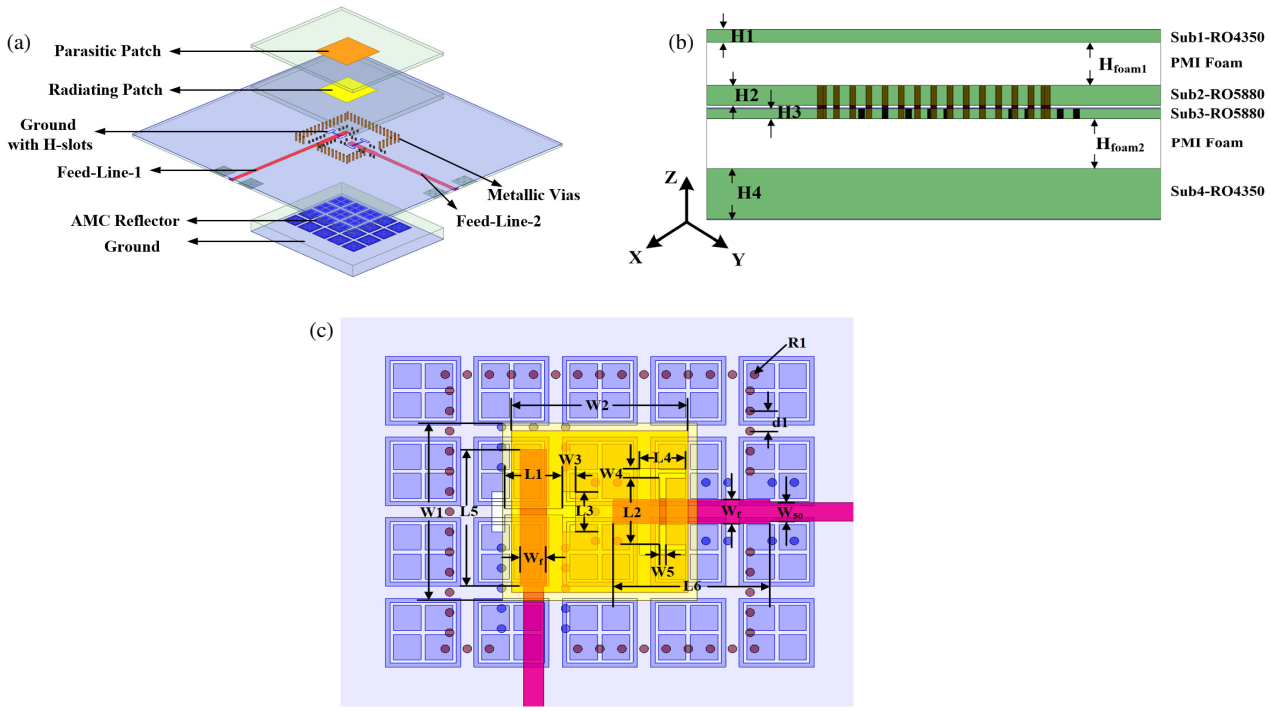

FIGURE 1. Configuration of the proposed antenna. (a) Perspective view. (b) Side view. (c) Top view.

2. ANTENNA CONFIGURATION

2.1. Antenna Geometry

The structure of dual-polarized antenna is shown in Fig. 1. The antenna is mainly composed of two parts, radiating part and AMC surface. It is designed based on four layers of substrates. The parasitic patch is put on the lower surface of substrate 1, and the radiating patch is on the upper surface of substrate 2. The upper surface of substrate 3 is the ground, and lower surface is two microstrip feed lines. The AMC is designed on the upper surface of substrate 4. Feed-line-1 is placed orthogonal to feed-line-2, and H-shaped slots are etched on the ground at the corresponding position to couple energy to the patch. Metallic vias are arranged around the feed lines and the patch. The port isolation and the cross-polarization level of the antenna can be optimized by these vias. The bottom AMC surface is constructed by a 4×5 array of AMC units.

2.2. Working Principle of AMC

With the electromagnetic wave incident perpendicularly, each patch results in an inductor L_1. The resulting inductance from the patch to the ground plane is represented by L_2. The gap between adjacent periodical patches provides a capacitor C_1. The equivalent circuit of AMC is shown in Fig. 2.

Z_1 and Z_2 are the equivalent impedances of the periodic patch and the substrate, respectively, which together produce parallel resonance:

$$Z_1 = j\omega L_1 + \frac{1}{j\omega C_1} \tag{1}$$

$$Z_2 = j\omega L_2 \tag{2}$$

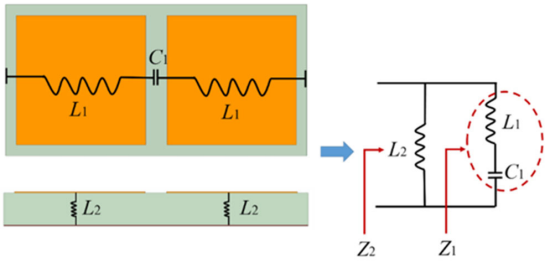

FIGURE 2. Equivalent circuit of AMC.

Hence, the total AMC surface impedance Z_S is expressed as:

$$Z_s = Z_1/Z_2 = j\omega L_2 \frac{1-\omega^2 L_1 C_1}{1-\omega^2 (L_1+L_2) C_1} \tag{3}$$

Z_0 is the wave impedance in free space, and the reflection coefficient Γ and the phase of reflection coefficient φ of the AMC can be calculated as:

$$\Gamma = \frac{Z_s - Z_0}{Z_s + Z_0} \tag{4}$$

$$j\varphi = \ln \frac{Z_s - Z_0}{Z_s + Z_0} \tag{5}$$

When the AMC surface is used as a reflecting plate, it is expected to achieve in-phase reflection characteristics. Therefore, the reflection coefficient Γ needs to be 1, so the $Z_0 = 0$. According to Equation (3), if $Z_s = \infty$, then:

$$1 - \omega^2 (L_1 + L_2) C_1 = 0 \tag{6}$$

The resonant frequency f_s can be expressed as:

$$\omega_r = \frac{1}{\sqrt{(L_1 + L_2)\, C_1}} \tag{7}$$

$$f_r = \frac{1}{2\pi\sqrt{(L_1 + L_2)\, C_1}} \tag{8}$$

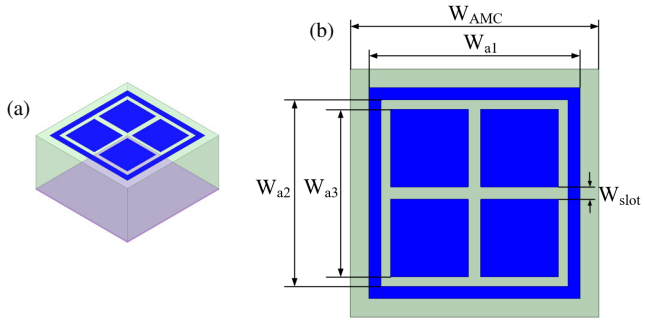

FIGURE 3. Structure of proposed AMC unit. (a) AMC unit. (b) AMC dimension.

2.3. Introduction of Proposed AMC Unit

The AMC unit consists of a large square ring and four small square patches, as shown in Fig. 3. The cross-slots and square ring are designed to introduce additional inductance to reduce the resonant frequency and minimize the size. The equivalent circuit model of the proposed AMC structure is shown in Fig. 4. The gaps between the adjacent periodic patches and the etched slots in the patches together provide a gap capacitance C_a, and one square ring patch and four square patches together provide an inductance L_a, A capacitance C_d is generated between the dielectric substrate and the floor. The resonant frequency can be calculated as follows:

$$f_r = \frac{1}{2\pi}\sqrt{\frac{1}{L_a}\left(\frac{1}{C_a} + \frac{1}{C_d}\right)} \tag{9}$$

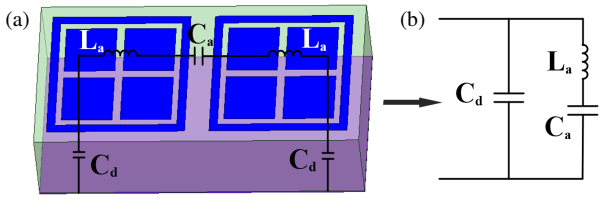

FIGURE 4. Equivalent circuit model of proposed AMC structures.

The ideal in-phase reflection bandwidth can be obtained corresponding to the operating frequency of the antenna by adjusting the parameters of the AMC structure. The simulated reflection phase performance of the AMC unit is shown in Fig. 5. The resonant frequency of proposed AMC is 9.38 GHz, which is the zero-reflection phase point. The effective reflection frequency band is 7.93–10.77 GHz, with a relative bandwidth of 30%.

The current distributions of the ground and E-field distribution of the antenna with and without AMC surface are shown in Fig. 6. When port 2 is excited, the antenna is horizontally polarized. When the AMC surface is loaded, the maximum current is

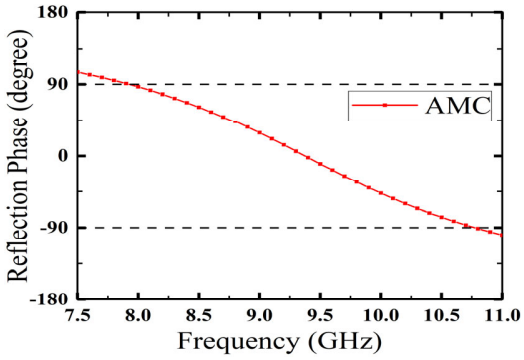

FIGURE 5. Reflection phase of the proposed AMC.

constrained around the H-shaped slot corresponding to port 2. The energy is basically coupled from this slot to the antenna, and the energy coupling between the slots is improved. In addition, due to the zero-phase reflection characteristic, the backward radiation wave is effectively reflected, thus the profile of antenna is reduced, and the gain is improved.

The microstrip antenna with AMC surface is compared with the antenna with a PEC reflector to verify the effectiveness of the AMC surface. The PEC reflector has the same size as the AMC surface, and the distance to the radiating patch is both 2 mm. The comparison of S-parameters between different antennas is shown in Fig. 7. The profile of the antenna with PEC reflector is 9.4 mm ($0.29\lambda_0$). The return loss deteriorates dramatically in the operating bandwidth when the profile is reduced to $0.23\lambda_0$. By loading the AMC surface between the microstrip antenna and the ground, the impedance bandwidth is greatly improved, which is larger than the antenna with PEC reflector at the profile of $0.29\lambda_0$, as shown in Fig. 7. Besides, the port isolation is also improved from 31 dB to 48 dB because the AMC surface limits the current between the slots on the ground. According to the above performance comparison, the introduction of AMC surface can significantly reduce the profile of antenna and improve the bandwidth and port isolation of antenna.

3. SIMULATED AND MEASURED RESULTS

The antenna is analyzed with the aid of ANSYS HFSS. The final dimensions of the antenna shown in above figures are listed in Table 1. The simulated performances of the optimized antenna are shown in Figs. 8–10. As shown in Fig. 8, the port iso-

TABLE 1. Antenna dimension (Unit: mm).

Parameters	$L1$	$L2$	$L3$	$L4$	$L5$	$L6$	$W1$
Value (mm)	2.6	3.3	2	2.1	6.8	7.1	8.8
Parameters	$W2$	$W3$	$W4$	$W5$	W_f	W_{50}	$r1$
Value (mm)	8	0.6	0.5	0.3	1.2	0.92	0.2
Parameters	$d1$	$H1$	$H2$	$H3$	$H4$	H_{foam1}	H_{foam2}
Value (mm)	1	0.508	0.813	0.308	2	1.7	2
Parameters	W_{AMC}	W_{a1}	W_{a2}	W_{a3}	W_{slot}		
Value (mm)	4	3.4	3	2.7	0.2		

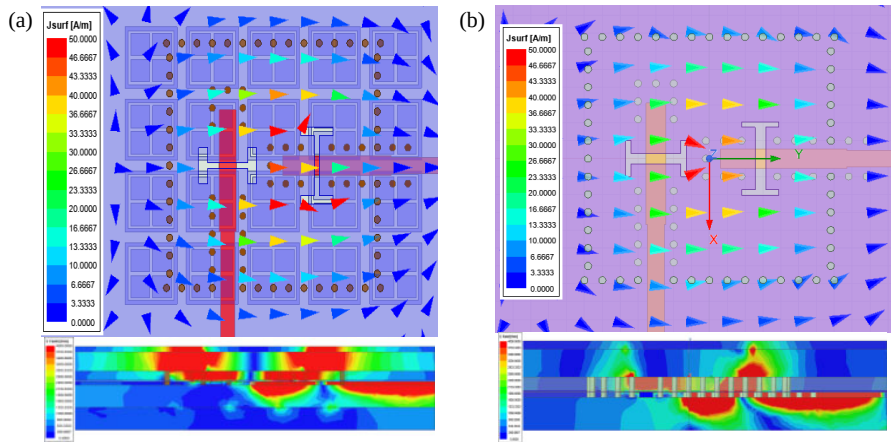

FIGURE 6. Current distributions of GND and E-field distribution. (a) With AMC. (b) Without AMC.

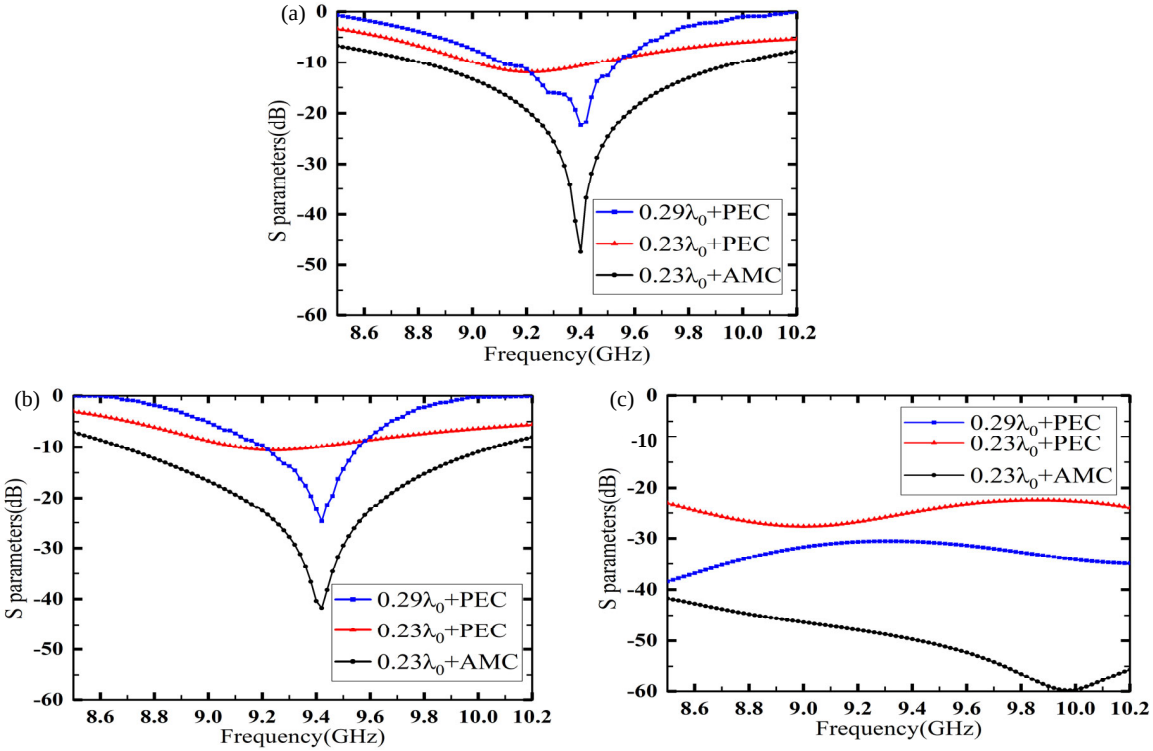

FIGURE 7. Comparison of S parameters with or without AMC surface. (a) Comparison of S_{11}. (b) Comparison of S_{22}. (c) Comparison of S_{21}.

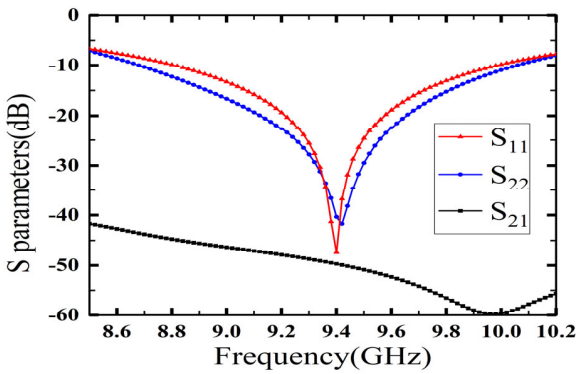

FIGURE 8. Simulated S parameters of the proposed antenna.

lation of two feedings is better than 48 dB in the frequency band of 9.3–9.5 GHz. $|S_{11}|$ is less than -10 dB over 8.81–9.99 GHz, and the relative impedance bandwidth is about 12.5%. The radiation patterns at 9.4 GHz are shown in the Fig. 9. The maximum gains of port 1 and port 2 can respectively achieve 7.24 dBi and 7 dBi, and the cross-polarization level is lower than -26 dB and -27 dB. As shown in Fig. 10, the average gains in band are about 7 dBi and 6.8 dBi, and a high efficiency about 96% is achieved.

The antenna was manufactured and measured. The antenna prototype and test environment are shown in Fig. 11 and Fig. 12. The prototype consists of four parts, including parasitic patch, two pieces of PMI foam, radiating patch with feed lines, and AMC surface. Each part has a screw installation space and

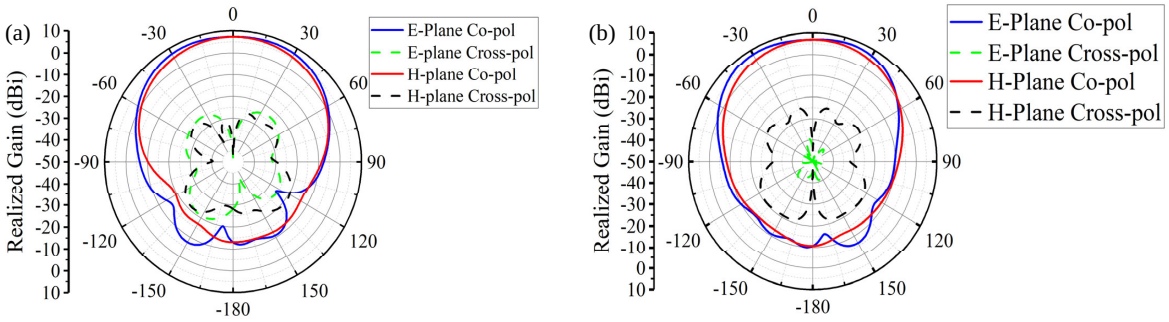

FIGURE 9. Simulated radiation patterns of the proposed antenna at 9.4 GHz. (a) Port 1. (b) Port 2.

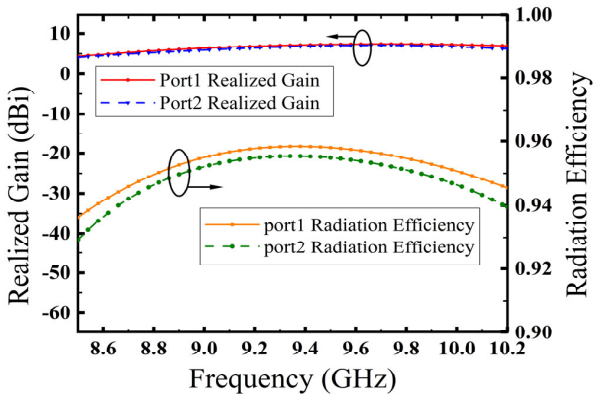

FIGURE 10. Simulated realized gain and radiation efficiency of the proposed antenna.

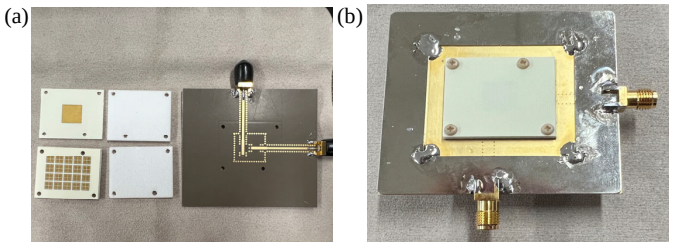

FIGURE 11. The prototype of antenna unit. (a) Detailed parts of prototype. (b) Assembled prototype.

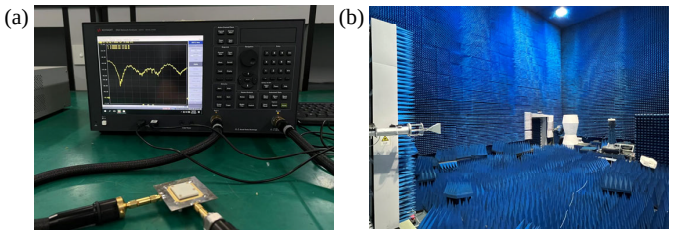

FIGURE 12. Antenna measurement conditions. (a) Measurement of S parameter. (b) Far-field chamber.

is connected by M2 nylon screws. A 0.5 mm thick square metal ring is independently processed and welded on the public ground in order to facilitate the installation of the surface mounting SMA connector and ensure the mechanical strength of the substrate. The inner core of the SMA is connected to the

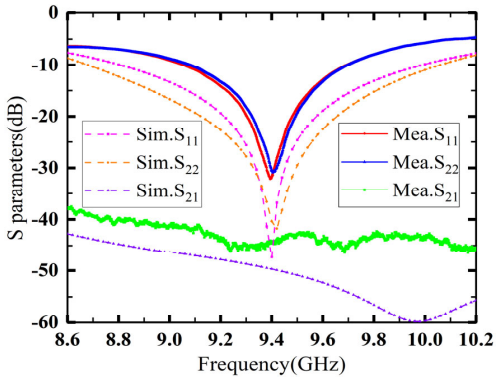

FIGURE 13. Measured and simulated S parameters.

microstrip feed line, and the outer wall is welded to the ground by soldering. The S-parameters of the antenna prototype are measured by KEYSIGHT E5071C, and the radiation patterns are measured in a far-field anechoic chamber.

The simulated and measured S-parameters of the antenna are shown in Fig. 13. The simulated impedance bandwidth for port 1 is 8.81 $\sim$ 9.99 GHz; the impedance bandwidth for port 2 is 8.68 $\sim$ 10.06 GHz; and the relative bandwidth is 12.5%. The measured results show that the bandwidth for $|S_{11}|$ and $|S_{22}|$ lower than -10 dB is 9.1 $\sim$ 9.78 GHz, and the relative bandwidth is about 7.23%. The measured port isolation is higher than 44 dB in the frequency band of 9.3–9.5 GHz and slightly less than 48 dB. The measured results are slightly worse than the simulated ones, which are mainly caused by the following reasons: First of all, the radiating parts of the antenna are painted on the RO5880 substrates. The thickness of substrates 2 and 3 is thin, and the hardness of the material of RO5880 is soft, so it is easy to warp during the manufacturing and installing process. Besides, the upper and lower parts of the substrates 2 and 3 are PMI foams. When the foam is squeezed during installation, it will also cause certain deformation, resulting in certain errors in the physical structure of the antenna. In addition, the welding accuracy of the surface mounting SMA is not high enough, and the link loss when the test system is used may also lead to reduced port isolation and impedance bandwidth.

The simulated and measured radiation patterns of port 1 and port 2 on the E and H planes at 9.4 GHz are shown in Fig. 14 and Fig. 15. The measured normal gain of vertical polarization is 6.98 $\pm$ 0.2 dBi. The measured normal gain of horizontal polarization is 6.5 $\pm$ 0.05 dBi. The measured value is

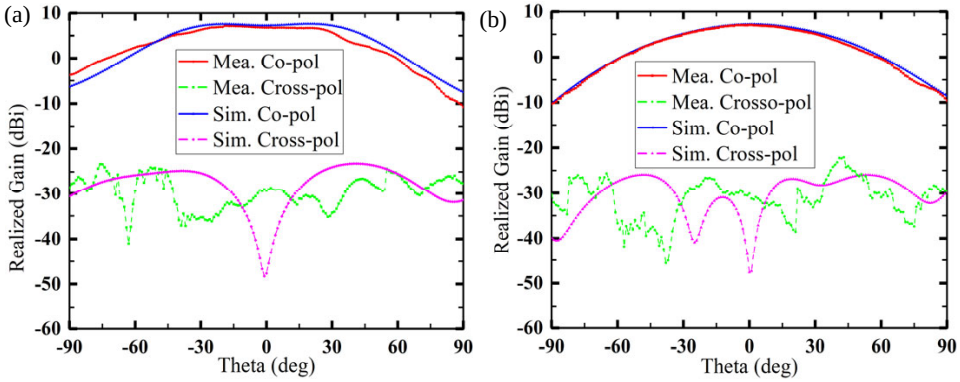

FIGURE 14. Vertical polarization radiation patterns at 9.4 GHz. (a) E plane. (b) H plane.

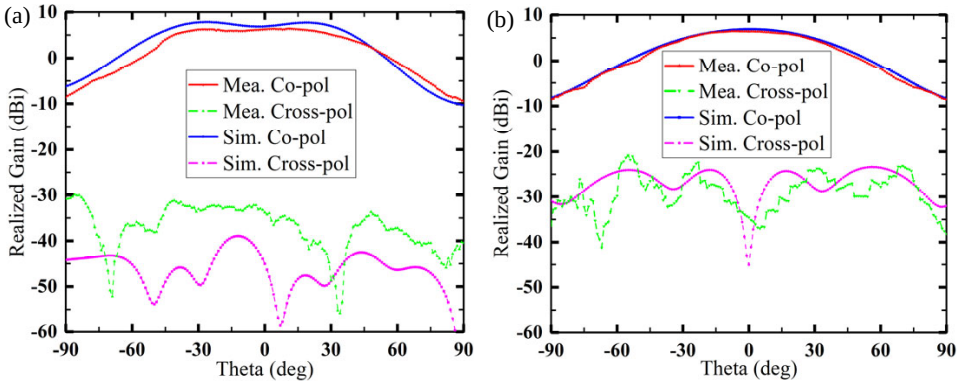

FIGURE 15. Horizontal polarization radiation patterns at 9.4 GHz. (a) E plane. (b) H plane.

TABLE 2. Comparison of the proposed antenna with some existing works.

Ref.	Type	Operating Frequencey (GHz)	Profile (λ_0)	Port Isolation (dB)	Cross Polarization (dB)
[5]	Microstrip ant	3.6	0.38	> 23	< -25
[6]	Microstrip ant	3.5	/	> 20	< -20
[7]	Microstrip ant	10	0.31	> 26	/
[8]	Microstrip ant	9.6	0.13	> 35	< -23
[9]	Microstrip ant	10	0.39	> 23	< -20
[14]	ME dipole with AMC	2.2	0.176	> 25	< -27
[18]	ME dipole with AMC	2.2	0.14	> 25	< -26
This work	Microstrip ant with AMC surface	9.4	0.23	> 48	< -26

slightly smaller than the simulation, which is mainly caused by the position deviation of the measured antenna and the horn antenna. In addition, the antenna connector will be subjected to the force generated by the test cable following the rotation of the turntable during measuring process, which may cause poor contact between the inner core of the SMA connector and the cable. Besides, the ambient noise of the chamber and the loss of the test system will also lead to errors in the measured and simulated results. The measured cross-polarization level of port 1 on E plane is better than -23 dB, and the cross-polarization level on H plane is better than -23 dB. The measured cross-polarization level of port 2 on E plane is better than -29 dB, and the cross-polarization level on H plane is better than -22 dB. This shows that the antenna has a relatively stable radiation pattern with low cross-polarization at 9.4 GHz, and the measured pattern is in good agreement with the simulated results.

The comparisons of this antenna with some other works are listed in Table 2. Compared with common dual-polarized microstrip antennas, the proposed antenna unit has a lower profile of $0.23\lambda_0$. Meanwhile, it has a high port isolation better than 48 dB and a cross-polarization level lower than -26 dB.

4. CONCLUSION

In this paper, a dual-polarized microstrip antenna with low profile and high port isolation based on AMC surface is proposed. By loading the AMC surface, the antenna profile is reduced from 9.4 mm to 7.3 mm, with the height reduction of 22%. Meanwhile, taking advantage of the AMC surface, the antenna has a port isolation better than 48 dB and a cross-polarization level lower than −26 dB. The proposed dual-polarized antenna will be a good choice for applications such as weather radar systems.

REFERENCES

[1] Gao, S., L. W. Li, M. S. Leong, and T. S. Yeo, "A broad-band dual-polarized microstrip patch antenna with aperture coupling," *IEEE Transactions on Antennas and Propagation*, Vol. 51, No. 4, 898–900, Apr. 2003.

[2] You, C., J. Choi, H. Ryu, D. Kim, G. Kim, and S. Kim, "Wideband dual-polarized on-board antenna for 5G mmWave mobile application," in *2022 14th Global Symposium on Millimeter-Waves & Terahertz (GSMM)*, 195–196, Seoul, Republic of Korea, 2022.

[3] Liu, H., A. Qing, Z. Xu, Z. Yu, and S. Zhang, "Design of physically connected wideband SIW cavity-backed patch antenna for wide-angle scanning phased arrays," *IEEE Antennas and Wireless Propagation Letters*, Vol. 20, No. 3, 406–410, Mar. 2021.

[4] Benny, S. and S. Sahoo, "Aperture fed microstrip dual polarization wide scan phased array antenna with mutual coupling reduction," *IEEE Access*, Vol. 12, 16 397–16 407, 2024.

[5] Hua, C., R. Li, Y. Wang, and Y. Lu, "Dual-polarized filtering antenna with printed jerusalem-cross radiator," *IEEE Access*, Vol. 6, 9000–9005, 2018.

[6] Yuan, H., F.-C. Chen, and Q.-X. Chu, "A wideband and high gain dual-polarized filtering antenna based on multiple patches," *IEEE Transactions on Antennas and Propagation*, Vol. 70, No. 10, 9843–9848, Oct. 2022.

[7] Liu, M. and W. Li, "An X-band dual-polarized microstrip phased array antenna with wide-angle scanning," in *2021 13th International Symposium on Antennas, Propagation and EM Theory (ISAPE)*, 1–3, Zhuhai, China, 2021.

[8] Wang, J., W. Wang, A. Liu, M. Guo, and Z. Wei, "Miniaturized dual-polarized metasurface antenna with high isolation," *IEEE Antennas and Wireless Propagation Letters*, Vol. 20, No. 3, 337–341, Mar. 2021.

[9] Yang, Y.-H., B.-Y. Liu, and S.-G. Zhou, "A wideband cavity-backed dual-polarized antenna for X-band applications," *IEEE Antennas and Wireless Propagation Letters*, Vol. 22, No. 4, 913–917, Apr. 2023.

[10] Zhang, X.-K., Y.-H. Ke, X.-Y. Wang, S.-C. Tang, and J.-X. Chen, "Broadband dual-polarized dielectric patch antenna with high isolation for full-duplex communication," *IEEE Antennas and Wireless Propagation Letters*, Vol. 22, No. 4, 878–882, Apr. 2023.

[11] Chou, H.-T., B.-A. Liu, S.-C. Chen, and Y.-J. E. Chen, "Dual-band dual-polarized microstrip patch antenna with parasitic elements for 5G antenna-in-package design at millimeter-wave frequencies," *IEEE Transactions on Components, Packaging and Manufacturing Technology*, Vol. 13, No. 11, 1778–1789, Nov. 2023.

[12] Kumari, S., Y. K. Awasthi, D. Bansal, R. Anand, P. K. Malik, and R. Singh, "A highly isolated tapered triangular dual-polarized multiband MIMO antenna for WLAN, C, X and Ku bands," *International Journal of Antennas and Propagation*, Vol. 2024, No. 1, 2356155, 2024.

[13] Liang, M.-S., Y. Zhou, X.-S. Yang, and P.-F. Wu, "A low-profile dual-polarized substrate integrated magneto-electric dipole MIMO antenna," *IEEE Antennas and Wireless Propagation Letters*, Vol. 22, No. 6, 1431–1435, Jun. 2023.

[14] Tan, M., Y.-H. Ren, C. Xu, Y.-Y. Wang, H.-D. Wu, and F.-W. Wang, "A low-profile wideband and dual-polarized antenna with AMC reflector," in *2022 International Conference on Microwave and Millimeter Wave Technology (ICMMT)*, 1–3, Harbin, China, 2022.

[15] Yuan, H. and F.-C. Chen, "A mixed decoupling scheme based on AMC and ADS for dual-polarized antenna array," *IEEE Transactions on Antennas and Propagation*, Vol. 71, No. 7, 6150–6155, Jul. 2023.

[16] Zhai, H., K. Zhang, S. Yang, and D. Feng, "A low-profile dual-band dual-polarized antenna with an AMC surface for WLAN applications," *IEEE Antennas and Wireless Propagation Letters*, Vol. 16, 2692–2695, 2017.

[17] He, X., B. Feng, and Q. Zeng, "A low-profile differentially feeding dual-polarized antenna using wideband AMC reflector," in *2018 IEEE International Conference on Signal Processing, Communications and Computing (ICSPCC)*, 1–4, Qingdao, China, 2018.

[18] Lv, J.-M., Z.-J. Guo, and Z.-C. Hao, "A low-profile differentially feeding dual-polarized antenna using wideband AMC reflector," in *2021 International Conference on Microwave and Millimeter Wave Technology (ICMMT)*, 1–3, Nanjing, China, 2021.